NASA/CR—2005-214033 AIAA–2006–0176

Numerical Investigation of Various Atomization Models in the Modeling of a Spray Flame

M.S. Raju
QSS Group, Inc., Cleveland, Ohio

November 2005

The NASA STI Program Office . . . in Profile

Since its founding, NASA has been dedicated to the advancement of aeronautics and space science. The NASA Scientific and Technical Information (STI) Program Office plays a key part in helping NASA maintain this important role.

The NASA STI Program Office is operated by Langley Research Center, the Lead Center for NASA's scientific and technical information. The NASA STI Program Office provides access to the NASA STI Database, the largest collection of aeronautical and space science STI in the world. The Program Office is also NASA's institutional mechanism for disseminating the results of its research and development activities. These results are published by NASA in the NASA STI Report Series, which includes the following report types:

- TECHNICAL PUBLICATION. Reports of completed research or a major significant phase of research that present the results of NASA programs and include extensive data or theoretical analysis. Includes compilations of significant scientific and technical data and information deemed to be of continuing reference value. NASA's counterpart of peer-reviewed formal professional papers but has less stringent limitations on manuscript length and extent of graphic presentations.

- TECHNICAL MEMORANDUM. Scientific and technical findings that are preliminary or of specialized interest, e.g., quick release reports, working papers, and bibliographies that contain minimal annotation. Does not contain extensive analysis.

- CONTRACTOR REPORT. Scientific and technical findings by NASA-sponsored contractors and grantees.

- CONFERENCE PUBLICATION. Collected papers from scientific and technical conferences, symposia, seminars, or other meetings sponsored or cosponsored by NASA.

- SPECIAL PUBLICATION. Scientific, technical, or historical information from NASA programs, projects, and missions, often concerned with subjects having substantial public interest.

- TECHNICAL TRANSLATION. English-language translations of foreign scientific and technical material pertinent to NASA's mission.

Specialized services that complement the STI Program Office's diverse offerings include creating custom thesauri, building customized databases, organizing and publishing research results . . . even providing videos.

For more information about the NASA STI Program Office, see the following:

- Access the NASA STI Program Home Page at ***http://www.sti.nasa.gov***

- E-mail your question via the Internet to help@sti.nasa.gov

- Fax your question to the NASA Access Help Desk at 301–621–0134

- Telephone the NASA Access Help Desk at 301–621–0390

- Write to:
  NASA Access Help Desk
  NASA Center for AeroSpace Information
  7121 Standard Drive
  Hanover, MD 21076

NASA/CR—2005-214033 AIAA–2006–0176

Numerical Investigation of Various Atomization Models in the Modeling of a Spray Flame

M.S. Raju
QSS Group, Inc., Cleveland, Ohio

Prepared for the
International Conference on Computational and Experimental Engineering and Sciences
cosponsored by the North Carolina A&T University, Simulation Technology Services Private, Ltd., U.S. Army Research Office, U.S. Army Asian Research Office, U.S. Air Force Asian Office of Aerospace Research and Development, The Indian National Academy of Engineering, and the National Science Foundation
Chennai, India, December 1–6, 2005
and the
44th Aerospace Sciences Meeting and Exhibit
sponsored by the American Institute of Aeronautics and Astronautics
Reno, Nevada, January 9–12, 2006

Prepared under Contract NAS3–00145

National Aeronautics and
Space Administration

Glenn Research Center

November 2005

Acknowledgments

The research funding for this work was provided by NASA Glenn Research Center with N.-S. Liu acting as the technical monitor. Special thanks to D.S. Crocker and B. Zuo for their enormous help during the integration of the atomization module into NCC. The author would like to thank John Marek, NASA Glenn Research Center, for his insightful comments and review of several papers over the last decade.

Available from

NASA Center for Aerospace Information
7121 Standard Drive
Hanover, MD 21076

National Technical Information Service
5285 Port Royal Road
Springfield, VA 22100

Available electronically at http://gltrs.grc.nasa.gov

Numerical Investigation of Various Atomization Models in the Modeling of a Spray Flame

M.S. Raju
QSS Group, Inc.
Cleveland, Ohio 44135

1 ABSTRACT

In modern aircraft and rocket engine combustors, the atomization characteristics of a fuel nozzle as defined by the spray dispersion angle, droplet-size and velocity distributions, and fuel vaporization play an important role in determining the combustor performance, e.g. the combustion efficiency, ignition and lean blowout conditions, exit temperature pattern, and emissions. The success of any spray calculation depends a great deal on the correct specification of the initial droplet conditions. However, the modeling of the atomization process is a very challenging task as it is influenced by a variety of factors: the aerodynamic liquid-gas interaction, the inner nozzle disturbances, the nozzle geometry, and the thermo-physical properties of fuel. So far in our previous spray computations, we have relied on either known experimental data or data generated from widely-used correlations in specifying the initial droplet conditions. In order to reduce some uncertainty associated with the specification of the initial droplet conditions, we have undertaken the task of integrating an atomization module into our spray calculation procedure of the national combustion code (NCC). The atomization module contains the following primary atomization models: (1) sheet breakup, (2) air blast, (3) blob jet, and (4) BLS (Boundary-Layer Stripping), together with the following secondary droplet breakup models: (1) Rayleigh-Taylor, (2) TAB (Taylor Analogy Breakup), and (3) ETAB (Enhanced Taylor Analogy Breakup). The paper provides complete details of various models contained in the atomization module. And it also summarizes the results from the study conducted to investigate the effect of various atomization models in the modeling of a spray flame.

2 INTRODUCTION

The state of the art in multi-dimensional spray combustion modeling, as evidenced by the level of sophistication employed in terms of modeling and numerical accuracy considerations, is also dictated by the available computer memory and turnaround times afforded by present-day computers. With the development of LSPRAY-II [1] and EUPDF-II [2], we have advanced the state of the art in multi-dimensional spray/gaseous combustion calculations by combining the novelty of the coupled CFD/spray/scalar Monte Carlo PDF (Probability Density Function) computations with the ability to run on massively parallel computers and unstructured grids. LSPRAY-II is a Lagrangian spray solver with a multi-injection capability and it is primarily designed to predict the flow, thermal and transport properties of a rapidly vaporizing

multi-component spray under both time-dependent and steady-state conditions; and EUPDF-II provides the solution for the species and temperature fields based on a PDF transport equation. Both of the modules are designed for massively parallel computing platforms and they could easily be coupled with any existing gas-phase CFD flow solver either independently of each other or in combination with both. Both of the solvers accommodate the use of an unstructured mesh with mixed elements of either triangular, quadrilateral, and/or tetrahedral type. Some major features of LSPRAY-II & EUPDF-II are [1-4]:

- In order to demonstrate the importance of chemistry/turbulence interactions in reacting sprays, we have extended the joint scalar Monte Carlo PDF (Probability Density Function) approach to the modeling of spray flames.
- Both of the modules accommodate the use of both unstructured grids and parallel computing and, thereby, facilite large-scale combustor computations involving complex geometrical configurations.
- In order to deal with modern gas-turbine fuels that are mixtures of many compounds, we have extended the spray formulation to the modeling of multi-component liquid fuels.
- In order to extend the applicability of the spray computations over a wide range of low-pressure conditions, we have completed the implementation of the variable liquid thermo-transport properties into our spray formulation.
- Both of the modules are designed in such a way so that they could easily be coupled with any other existing CFD code.
- While LSPRAY-II can be used in the calculation of both steady as well as unsteady computations, EUPDF-II is primarily designed for the steady-state calculations.
- We have developed and implemented several numerical convergence techniques such as local time-stepping and various other averaging schemes in order to accelerate convergence to a steady state.
- The spray module has a multi-liquid and multi-injection capability.
- Its application has been demonstrated in various important NASA projects: Ultra-Efficient Engine Technology (UEET), Pulse Detonation Combustion Technology (PDCT), & Rotary Combustion Engine Technology Enablement Project (RCETEP).

In order to reduce the uncertainty associated with the specification of the initial droplet conditions, we have undertaken the task of integrating an atomization module into our spray calculation procedure. The atomization module is based on some recent progress made in the modeling of the atomization process [5-12] and was developed by CFDRC Inc. [11] in collaboration with the university of Wisconsin (UW) [9-10]. The atomization process can be broadly classified into two breakup regimes: (1) within the injector, the inner-nozzle disturbances due to cavitation may lead to the formation of a fragmented liquid, and (2) on the outside of the nozzle exit, the aerodynamic forces are responsible for the disruption of the liquid into ligaments, fragments, and tiny droplets [7-8]. The approach taken here ignores the internal-injector processes but uses available knowledge of the external spray characteristics [5]. The breakup of the liquids due to aerodynamic forces is a result of hydrodynamic instabilities on the liquid-gas interface such as either Rayleigh-Taylor or Kelvin-Helmholtz instabilities [5, 7-8]. The Rayleigh-Taylor instability is due to inertia of the denser fluid opposing the system acceleration in a direction perpendicular to the interface of the denser fluid and the Kelvin-Helmholtz instability is caused by the viscous forces due to the relative motion of the fluids [7-8]. Based on a linear instability analyses of a 2D viscous incompressible fluid moving thorough an inviscid incompressible gas, Reitz and Bracco [5] characterized the break-up regimes to be four-fold: (1) Rayleigh breakup, (2) first wind-induced breakup, (3) second wind-induced breakup, (4) atomization. In the first two regimes, drops of sizes greater than or equal to the nozzle diameter are produced at distances far from the nozzle exit. The last two regimes are more important to the atomization studies of our interest and

drops of sizes smaller than the nozzle diameter are produced near the nozzle exit. The knowledge gained from the instability analyses of various kinds [5, 9-10] is combined with some experimental observations to form the basis for the atomization and droplet breakup modeling of liquid sprays. As the atomization of the injected liquid and the subsequent breakup of drops are distinguishable processes within a dense spray, the jet breakup is modeled by making use of a drop representation approach in which discrete parcels of liquid are injected in the form of blobs with a characteristic size representative of the nozzle diameter instead of tracking an actual intact liquid core at the nozzle exit. In the case of a planar or conical liquid sheet, the discrete parcels essentially represent liquid ligaments. Before atomization, the discrete parcels stay inside of the liquid core or sheet but after atomization they move independently. The breakup criterion, atomization rate, drop size and velocity and the location of the newly formed droplets is primarily determined based on an instability analysis of the equations derived from the conservation of mass, momentum and energy. The analysis of the jet or sheet breakup into ligaments or smaller droplets, the stripping of the liquid into fragments or smaller droplets, the formation of smaller droplets from further breakup of ligaments or fragments is described under the classification of a primary atomization breakup model. Once the droplets are formed after atomization they may further breakup into smaller droplets based on a secondary droplet breakup mechanism while their behavior is tracked by a Lagrangian spray solution procedure as described in Ref. [1]. Further details of our spray solution procedure used in the spray computations can be found in [1-4].

Here we attempt to provide complete details of both the primary atomization breakup models as well as the secondary droplet breakup models of the atomization module. Also, we summarize the results from several test runs involving a single experimental case of McDonnell-Samuelsen [23]. However, the purpose of this exercise is not for any validation but it was designed primarily as a debugging platform for assessing the differences between various models. The designed test matrix consisted of a total of twenty runs resulting from all the available joint combinations of various primary atomization and secondary droplet breakup models.

3 DETAILS OF THE PRIMARY SPRAY ATOMIZATION MODELS

3.1 Sheet Breakup Primary Atomization Model (Likely Application: Pressure Swirl Atomizer)

Here, we summarize the details of the sheet breakup model taken from Schmidt et al [12]. The growth of an infinitesimal disturbance as given by

$$\eta \;=\; \eta_o \, exp(ikx \;+\; \omega t) \tag{1}$$

was analyzed based on a linear stability analysis of a two-dimensional, viscous, incompressible liquid sheet of thickness $2h$ which moves through an inviscid, incompressible gas medium. This was analyzed in a coordinate system moving with the sheet with a relative velocity of U where η_o is the initial wave amplitude, k $(= 2\pi/\lambda)$ is the wave number, and $\omega \;=\; \omega_r \;+\; i\omega_i$ is the complex growth rate. The most unstable disturbance responsible for the sheet breakup is denoted by Ω.

Based on the linearized liquid and gas continuity and momentum equations subject to the linearized boundary conditions at the gas and liquid interfaces, a sinuous mode dispersion relation was obtained by [13],

$$\begin{aligned} &\omega^2[tanh(kh) + Q] + \omega[4\nu_l k^2 tanh(kh) + 2iQkU] + \\ &4\nu_l^2 k^4 tanh(kh) - 4\nu_l^2 k^3 l \; tanh(lk) - QU^2k^2 + \tfrac{\sigma k^3}{\rho_l} \;\; = 0 \end{aligned} \tag{2}$$

where $Q \;=\; \rho_g/\rho_l$, $l^2 \;=\; k^2 \;+\; \omega/\nu_l$, and U is the relative velocity between the liquid and gas. Inviscid analysis also indicates that for low gas Weber number ($We = \rho_g h U^2/\sigma$) flows, long waves tend to grow leading to liquid sheet breakup but for higher Weber numbers, short waves produce a maximum growth rate

followed by breakup. The critical Weber number that leads to the transition from the long wavelength regime to the short wavelength regime was shown to be $We_g = 27/16$. For most modern fuel injection systems, the film Weber number is well above this critical limit. The growth rate for the sinuous mode, ω_r, based on an order of magnitude analysis of the dispersion relation yields,

$$\begin{aligned} \omega_r &= -\frac{2\nu_l k^2 tanh(kh)}{tanh(kh)+Q} \\ &\quad + \sqrt{\frac{4\nu_l^2 k^4 tanh^2(kh) - Q^2U^2k^2 - [tanh(kh)+Q](-QU^2k^2 + \sigma k^3/\rho_l)}{tanh(kh)+Q}} \end{aligned} \tag{3}$$

For short waves in the limit of $Q << 1$ for high-speed sheets, it yields

$$\omega_r = -2\nu_l k^2 + \sqrt{4\nu_l^2 k^4 + QU^2k^2 - \frac{\sigma k^3}{\rho_l}} \tag{4}$$

Following Dombrowski & Johns [15], the sheet disintegration leads to the formation of ligaments once the unstable waves reach a critical amplitude and Eq. (4) shows that the growth rate of short waves is independent of the sheet thickness. The corresponding breakup time τ and the breakup length L are given by:

$$\eta_b = \eta_o \, exp(\Omega\tau) \quad => \quad \tau = \frac{1}{\Omega} ln \frac{\eta_b}{\eta_o} \tag{5}$$

$$L = V\tau = \frac{V}{\Omega} ln(\frac{\eta_b}{\eta_o}) \tag{6}$$

where Ω is the maximum growth rate as determined by Eq. (4), the term $ln(\frac{\eta_b}{\eta_o})$ has an assigned value of 12 as suggested by Dombrowski & Hooper [14], and V is the absolute velocity of the liquid.

The initial diameter of the ligaments is derived from a mass balance relationship. For long waves, it is assumed that the ligaments are formed from tears in the sheet once per wavelength and the resulting diameter is given by,

$$d_L = \sqrt{\frac{8h}{K_s}} \tag{7}$$

where K_s is the wave number corresponding to the maximum growth rate Ω as obtained from Eq. (3) and the film thickness, h, is calculated from the breakup length, L, the radial distance from the centerline to the mid-line of the liquid sheet at the atomizer exit, r_o, and the spray angle, θ, as follows: $h = \frac{\dot{m}}{2\pi\rho_l V(r_o + Lsin(\theta/2))}$. For short waves, the ligament diameter is independent of the liquid sheet thickness and is assumed to be proportional to the wave length associated with the maximum growth rate Ω as follows: $d_L = \frac{2\pi C_L}{K_s}$ where the ligament constant, C_L, is equal to 0.5.

For both long and short waves, Dombrowski & Johns [15] developed a linear stability analysis for the further breakup from ligaments to droplets based on the Weber's analysis on capillary instability. The analysis shows that the breakup occurs when the amplitude of the unstable waves nears the radius of the ligament. And the corresponding most unstable wavenumber, K_L, is given by:

$$K_L d_L = [\frac{1}{2} + \frac{3\mu_L}{2\sqrt{\rho_L \sigma d_L)}}]^{-\frac{1}{2}} \tag{8}$$

This analysis thus yields the most probable droplet size based on a simple mass balance calculation where $d_D^3 = 3\pi d_L^2 / K_L$.

3.1.1 Application to pressure swirl atomization

For the pressure swirl atomizer, the initial injector exit velocity and liquid sheet thickness are calculated following the approach of Schmidt et al [12]. It assumes a uniform velocity profile for the initial liquid velocity, V, as given by,

$$V = max\{0.7, \frac{4\dot{m}}{\pi d_o^2 \rho_l cos\theta}\sqrt{\frac{\rho_l}{2\Delta p}}\}\sqrt{\frac{\Delta p}{\rho_l}} \tag{9}$$

where $\dot{m}$ and θ are the measured mass flow rate and spray angle, respectively, d_o is the injector exit diameter, and Δp is the pressure drop in the injector. Once V is known, the corresponding axial component of the sheet velocity is calculated via $u = V\ cos\theta$. And the initial sheet thickness h_o is calculated from the conservation of mass:

$$\dot{m} = \pi \rho_l u h_o (d_o - h_o) \tag{10}$$

At the point of primary breakup, the actual drop size is chosen from a Rosin-Rammler distribution with the mean size as given by d_D of the sheet breakup model. Further movement of the droplets is tracked by making use of a Lagrangian formulation.

3.2 Blob Jet Primary Atomization Model (Likely Application: Single-Orifice Nozzles)

Here we summarize the details of the blob jet primary atomization model taken from Reitz & Bracco [5] and Reitz [16,9]. It applies for a cylindrical liquid jet issuing into an incompressible gas. The following dispersion relation was obtained based on the stability analysis of a cylindrical liquid surface subjected to linear perturbations:

$$\begin{aligned}\omega^2 = 2\nu_l k^2 \omega\{\tfrac{I_1'(ka)}{I_0(ka)} - \tfrac{2kl}{k^2+l^2}\tfrac{I_1(ka)}{I_0(ka)}\tfrac{I_1'(la)}{I_0(la)}\} &= \tfrac{\sigma k}{\rho_l a^2}(1-k^2a^2)\{\tfrac{l^2-k^2}{l^2+k^2}\}\tfrac{I_1(ka)}{I_0(ka)} \\ &+\tfrac{\rho_2}{\rho_1}(U - i\omega l k)^2 k^2 \{\tfrac{l^2-k^2}{l^2+k^2}\}\tfrac{I_1(ka)}{I_0(ka)}\tfrac{K_0(ka)}{K_1(ka)}\end{aligned} \tag{11}$$

where I_0, I_1, and K_0, K_1 are the modified Bessel functions of the first and the second kinds.

Reitz [16,9] generated curve-fits of numerical solutions to Eq. (11) for the maximum growth rate ($\omega = \Omega$) and the corresponding wavelength ($\lambda = \Lambda$):

$$\frac{\Lambda}{a} = 9.02\frac{(1+0.45Z^{0.5})(1+0.4T^{0.7})}{(1+0.87We_2^{1.67})^{0.6}} \tag{12}$$

$$\Omega\{\frac{\rho_l a^3}{\sigma}\}^{0.5} = \frac{0.34+0.38We_2^{1.5}}{(1+Z)(1+1.4T^{0.6})} \tag{13}$$

where $Z = \frac{We_1^{0.5}}{Re_1}$, $T = ZWe_2^{0.5}$, $We_1 = \frac{\rho_1 U^2 a}{\sigma}$, $We_2 = \frac{\rho_2 U^2 a}{\sigma}$, and $Re_1 = \frac{Ua}{\nu_1}$. A core region is predicted with the blob injection method because there is a region of large discrete liquid parcels near the nozzle. Based on the jet stability theory, new drops are formed from a parent drop or blob. It is assumed that small droplets (with radius, r) are formed from the parent drops (with radius, a) with drop size proportional to the wavelength of the fastest-growing or most-unstable wave,

$$\begin{aligned} r &= B_o\Lambda \qquad (if\ B_o\Lambda \le a)\ \ or \\ r &= min\{(3\pi a^2 U/2\Omega)^{0.33},\ (3a^2\Lambda/4)^{0.33}\}\ \ (if\ B_o\Lambda > a,\ one\ time\ only)\end{aligned} \tag{14}$$

where $B_o = 0.61$ according to Reitz [16,9]. In the above, it is assumed for the ($B_o\Lambda \le a$) condition that small droplets are formed with the dropsize proportional to the wavelength of the fastest growing mode and the second ($B_o\Lambda > a$) condition applies to drops larger than the jet and it assumes that the jet disturbance has

frequency $\Omega/2\pi$ (a drop is formed each wave period) or that the drop size is determined from the volume of liquid contained under one surface wave. And the rate of change of droplet radius due to breakup is given by,

$$da/dt \quad = \quad -(a-r)/\tau \qquad (r \leq a) \tag{15}$$

where τ is the breakup time, $\tau = 3.726 B_1 a/\Lambda\Omega$, and the value for the breakup time constant, B_1, depends on the injector characteristics and its value ranges between 1.732 to 40. And $a(t = t_o) = a_o$ is the initial drop radius at time, t_o.

After the breakup, a new parcel containing product drops of size, r, is created and added to the computations [9]. This was done as long as the mass of the liquid removed from the parent ($\rho_l 4\pi(a_o^3 - a^3)/3$) reached or exceeded 3% of the average injected parcel mass and if the number of product drops is greater than or equal to the number of parent drops [9]. While waiting for sufficient product drops to accumulate, the parent drop number was adjusted so that $Na^3 = N_o a_o^3$ but the parent drop number, N_o, was then restored following the creation of the new product parcel [9].

In the case of ($B_o\Lambda > a$), the parent parcel was replaced by a new parcel containing drops with size given by Eq. 14 after a time equal to τ (with $N = N_o a_o^3/r^3$) [9]. This breakup procedure was allowed only once for each injected parcel [9].

Validation of the model for a single hole orifice in a typical diesel engine was demonstrated by Reitz and Diwaker [10] and Reitz [16,9].

3.3 Air Blast Primary Atomization Model (Likely Application: Air Blast Atomizers)

The air blast atomization model is essentially based on the idea of pressure-swirl atomization model (Section 3.1.1) as the primary atomization of an air blast injector is based on the aerodynamic analysis involving the Kelvin-Helmholtz instability of a liquid jet in an incompressible gas. It, however, differs from the pressure-swirl atomization model in the determination of the initial sheet velocity and thickness as given by

$$V_{sheet} \quad = \quad \alpha V_l \; + \; (1-\alpha) V_g \tag{16}$$

$$\delta \quad = \quad r\big[1 - \sqrt{1 - \frac{\dot{m}}{\pi r^2 \rho V_{sheet}}}\big] \tag{17}$$

where α has a value of 0.12 to 1 depending on the fuel filmer characteristics, r is the radius of the fuel filmer, and $\dot{m}$ is the fuel flow rate. The continuous annular sheet is represented by a finite number of point injectors located randomly along the circular ring of the liquid sheet.

3.4 Modified BLS Primary Atomization Model (Likely Application: Liquid Jet in a Cross Flow)

Here we summarize the details of the BLS atomization model taken from Khosla and Crocker [11]. In this model both surface shear breakup and column breakup modes are included. Before column breakup, fragments may be formed due to boundary layer stripping depending on the local Weber number and q ($= \rho_l u_l^2/\rho_g u_g^2$). When the jet reaches the column breakup time, the entire jet breaks into fragments. It also allows for further breakup of the fragments based on a modified boundary layer stripping. And it is followed by a final breakup step based on the Rayleigh-Taylor secondary droplet breakup model.

Fragments are stripped from the liquid column if the We_g satisfies the following criteria:

$$\begin{aligned} We_g &> 50 Re_g^{1/2}\, q^{-1/0.81}\ and \\ We_g &> 15 \end{aligned} \tag{18}$$

where

$$Re_g = \rho_g d_j u_g / \mu_g$$
$$we_g = u_g^2 d_j \rho_g / \sigma_l$$

where Re_g and We_g are based on the gas velocity component normal to the liquid jet direction instead of the relative velocity. If column stripping does occur, the amount of mass removed from the column is given by,

$$M_{shed} = \frac{3}{4}\pi d \rho_l \frac{t_b}{t^\star} u_{rel} A \alpha \sqrt{\frac{\pi d}{4}} \Delta t \tag{19}$$

where,

$$A = \left[\frac{\rho_g}{\rho_l}\right]^{1/3} \left[\frac{\mu_g}{\mu_l}\right]^{1/3} \tag{20}$$

$$\alpha = \left[\frac{8\mu_l}{3 A u_{rel} \rho_l}\right]^{1/2} \tag{21}$$

$$t^\star = \frac{d_o \sqrt{\frac{\rho_l}{\rho_g}}}{u_g} \tag{22}$$

where t_b is the liquid column drop lifetime. The addition of the factor $t^\star/t_b$ causes the shedding rate to increase essentially linearly with distance away from the injection location. This accounts for the lack of shedding close to the injection location and the subsequent buildup of shedding over the life of the liquid column. The shed drop SMD (Sauter Mean Diameter) is given by

$$SMD = 3.1 \frac{t_b}{t^\star} d^{1/2} \left[\frac{\rho_l}{\rho_g}\right]^{1/4} \left[\frac{\mu_l}{u_{rel}\rho_l}\right]^{1/2} \tag{23}$$

The $t_b/t^\star$ factor is included with the effect of producing smaller drops near the injection location. However, $t_b/t^\star$ is limited to a minimum value of 2.5 which is never exceeded for some cases. The amount of mass shed is tracked and 10 new parcels are created when the cumulative shed mass after a time step exceeds 1% of the mass of the parcel. Each parcel is allocated an equal amount of the shed mass and the size for each new parcel is selected randomly from a uniform distribution between 0.4 and 1.6 times the mass mean diameter, MMD. And the drop velocities were given by

$$u_d = u_p + O.3(RND - 0.2)(u_g - u_p) \tag{24}$$

$$v_d = v_p + +0.3(RND - 0.2)(v_g - v_p) \tag{25}$$

$$w_d = w_p + 0.25(RND - 0.5)(u_{rel} - w_p) \tag{26}$$

where RND is a random number. Column stripping occurs, assuming the above criteria are met, until the column breakup time is exceeded. Parcels created through the column stripping mechanism are considered to be fragments which may undergo further breakup as discussed below. First, though, the column breakup mechanism, which also produces fragments, is described. The liquid jet column breakup time is given by

$$t_b = A_b We^{0.62} t^\star \tag{27}$$

The constant, A_b, has a value of 25. Since the present model includes a fragment breakup step after the column breakup, the We dependence for the breakup onset was retained.

After the column breakup time is reached, the column is broken into 18 new parcels with $MMD = 0.45 d_j$. The new parcels are also designated as fragments. The size of the fragments still tend to be large, so the ultimate drop size from the primary breakup process is mostly determined from the fragment breakup process. The size distribution is the same as described above for the column stripping. The cross flow and normal velocity components are the same as Eqs. (24) and (25). The lateral velocity component is given by

$$w_d = w_p + 0.1(RND - 0.5)(u_{rel} - w_p) \tag{28}$$

Fragments are further broken into small drops according to a modified version of the boundary layer stripping model based on the following criteria,

$$\begin{aligned} We_g &> \sqrt{Re}\ and \\ We_g &> 15 \end{aligned} \tag{29}$$

where

$$we_g = u_{rel}^2 d_d \rho_g / \sigma_l$$
$$Re_g = \rho_g d_d u_{rel} / \mu_g$$

The criteria are generally the same as for column stripping except that the dependence on q is not needed. Also note that We and Re are now determined using the relative velocity instead of the cross flow velocity. Again, the mass shed from a fragment in a time step and the SMD are given by

$$M_{shed} = 1.2\pi d \rho_l u_{rel} A \alpha \sqrt{\frac{\pi d}{4}} \Delta t \tag{30}$$

$$SMD = 3.6 d^{1/2} \Big[\frac{\rho_l}{\rho_g}\Big]^{1/4} \Big[\frac{\mu_l}{u_{rel}\rho_l}\Big]^{1/2} \tag{31}$$

where A and a are given by Eqs. (20) and (21), respectively. The new droplet velocities are given by Eqs. (24), (25), and (28). The broken fragments produce 3 new parcels with size distribution the same as described above when the shed mass from the fragment exceeds 20% of the fragment mass. A fragment can continue to breakup until it no longer meets the criteria of Eq. (29) or until its size is lower than the newly created drops. Once the fragment breakup process is complete, drops may breakup further based on a Rayleigh-Taylor secondary breakup method.

Khosla and Crocker [11] applied the model to predict the properties of Jet A-1 kerosene fuel injected into a cross-flowing air stream.

4 DETAILS OF SECONDARY DROPLET BREAKUP MODELS

Recent studies by Reitz et al [19, 16] have examined the breakup of single droplets moving in a transverse, high-velocity air jet. The high-speed photography provided new insights into the details of the breakup mechanism of a single drop. The droplet breakup regimes are classified as bag, stripping (shear) and catastrophic (surface wave) based on an increasing size of Weber number. In the bag breakup mode (at low Weber number), the drop is flattened by the aerodynamic pressure, then turned inside out, forming a thin hollow bag which is tied together with a circular belt-like structure on the windward side. The bag eventually bursts into smaller liquid fragments, whereas the belt decays into larger ligaments and droplets. In the stripping regime thin sheets or ligaments of fluid are continuously shed from the periphery of the distorting

parent drop as a consequence of a K-H instability, causing these sheets to disintegrate into tiny droplets. This process always leaves a coherent residual parent drop. The catastrophic drop breakup takes place in two stages leading to a collection of larger and tiny product droplets: Large amplitude long-wavelength waves caused by drop deceleration induce a R-T instability on the flattened drop which leads to a breakup into large product droplets, while at the same time short surface waves induce a K-H instability on the windward side of the parent drop resulting in a collection of much smaller product droplets. In diesel or other high-pressure gas-turbine sprays the droplets span a wide range of velocities and hence Weber numbers, and thus it is expected that all three droplet breakup mechanisms are relevant in the breakup modeling.

In what follows, we provide some details of the secondary droplet breakup models contained in the CFDRC/UW atomization module: (1) Rayleigh-Taylor, (2) TAB, and (3) ETAB. These details are taken from [16-21, 6-8].

4.1 Rayleigh-Taylor Secondary Droplet Breakup Model

Here we summarize the Rayleigh-Taylor secondary breakup model developed by Patterson and Reitz [21]. It is based on the analysis developed by Taylor [17,21] that accounts for the disturbances caused by droplet deceleration. In the Rayleigh-Taylor breakup mechanism, the breakup wavelength, Ω, is given by

$$\Omega \;=\; 0.2\pi\sqrt{3\sigma/|\dot{u}_d|(\rho_l-\rho_g)} \tag{32}$$

where $\dot{u}_d$ is the drop deceleration ($=\frac{3}{4}\frac{c_d\rho_g U^2}{\rho_l d}$, c_d is the aerodynamic drag coefficient, U is the drop relative velocity, & d is the drop diameter). Furthermore, the breakup wavelength Ω is limited by

$$\Omega \;=\; max(0.8d,\Omega)[1+0.2(RND-0.5)] \tag{33}$$

and the breakup time, $t_{b,RT}$, is given by

$$t_{b,RT} \;=\; c_{freq}\sqrt{0.5\sqrt{\sigma}(\rho_l+\rho_g)(\frac{3}{|\dot{u}_d|(\rho_l-\rho_g)})^{1.5}} \tag{34}$$

However, the value assigned for the constant, c_{freq}, depends on the droplet classification - parent, product, or default. For more details, one can refer to Patterson and Reitz [21]. After the breakup, no new drop parcels are created and there is no change in velocities between the parent and product drops. However, the drop number in a given parcel changes to $n_{product}$ as given by $n_{parent}(d_{parent}/\Omega)^3$ due to the change in the sizes between the parent and product drops.

4.2 The TAB Secondary Droplet Breakup Model (Likely Application: Lenticular-Shaped Droplet Deformations)

In an attempt to provide a description of the droplet and jet disintegration in the modeling of diesel sprays, O'Rourke & Amsden introduced the TAB model [6]. Here we summarize the TAB model taken from [7-8].

The TAB breakup model is based on Taylor's analogy between an oscillating, distorting drop and a spring-mass system. A detailed analysis of this model together with a discussion of its numerical implementation can be found in [6 & 22]. In this model, the drop motion is governed by a linear ordinary differential equation for a forced, damped harmonic oscillator. The forcing term is given by the aerodynamic droplet-gas interaction, the damping is due to the liquid viscosity and the restoring force is supplied by the surface tension. The parameters and constants have been determined partly from theoretical considerations and partly from experimental observations.

The TAB model describes the distortion of the drop by the deformation parameter, $y \;=\; 2x/a$, where x denotes the increase in the radius of the equator from its equilibrium position and a is the drop radius. The equation for the distortion parameter y is given by

$$\ddot{y} \; + \; \frac{5\mu_l}{\rho_l a^2}\dot{y} \; + \; \frac{8\sigma}{\rho_l a^3}y \; = \; \frac{2\rho_g |U|^2}{3\rho_l a^2} \tag{35}$$

Assuming a constant relative drop-gas velocity, U (which is satisfied in the numerical solution process during a given time step), the solution to Eq. (35) is given by

$$y(t) \; = \; \frac{We}{12} \; + \; e^{\frac{-t}{t_d}}\big(\big[y(o) \; - \; \frac{We}{12}\big]cos\omega t \; + \; \big[\frac{\dot{y}}{\omega} \; + \; \frac{y(0) - \frac{We}{12}}{\omega t_d}\big]sin\omega t\big) \tag{36}$$

where $We \; = \; \rho_g a U^2/\sigma$ and

$$t_d \; = \; \frac{2\rho_l a^2}{5\mu_l} \tag{37}$$

$$\omega^2 \; = \; \frac{8\sigma}{\rho_l a^3} \; - \; \frac{1}{t_d^2} \tag{38}$$

In this model, it is assumed that a necessary condition for drop breakup is reached when $We \; > \; We_{crit}$. And the value for the critical Weber number is determined experimentally to be 6. For an inviscid liquid with initial deformation conditions $y(0) \; = \; \dot{y}(0) \; = \; 0$, the solution to Eq. (35) reduces to $y(t) \; = \; We(1 \; - \; cos\omega_o t)/12$, where $\omega_o^2 \; = \; \frac{8\sigma}{\rho_l a^3}$ [8]. Consequently, the breakup occurs when $y(t) \; > \; 1$. The drop size after breakup is determined by an energy balance equation between the parent and the product droplets which equates the surface energies of parent drops with the energies of product drops due to oscillation and distortion. Also, the product droplets are initially equipped with the additional deformation velocity $\dot{x} \; = \; \alpha\dot{y}/2$, which acts normal to the path of the parent drop and is responsible for the formation of the spray angle.

One major advantage of this model is that it is based on a simple linear equation and it can be used effectively to describe the lenticular-shaped droplet deformations as observed in the experiments of [20 & 18].

4.3 The ETAB Secondary Droplet Breakup Model (Likely Application: High-Pressure Diesel Engine)

Here we provide some details of the ETAB model taken from Tanner [7-8]. The ETAB model is based on the following modifications to the standard TAB model: (1) the droplet disintegration is modeled via an exponential law which relates the mean product droplet size to the breakup time of the parent drop; and (2) an energy balance consideration between the parent and product droplets yields an expression for the normal velocity component of the product droplet.

When the breakup condition of $We \; > \; We_{crit} = 6$ and $y(t_{bu}) \; = \; 1$ is met, then the parent drop breaks up into a collection of product droplets, subject to a size distribution function which, in general, depends on the breakup mechanism. In the ETAB model, the rate of product droplet generation, dn(t)/dt, is given by

$$\frac{dn(t)}{dt} \; = \; 3K_{br}n(t) \tag{39}$$

where $n(t) \; = \; m_0/\bar{m}(t)$ and m_0 is the mass of the parent drop and $\bar{m}$ the mean mass of the product droplet distribution. Utilizing the fact that $dn/dt \; = \; -(m_0/\bar{m}^2)(d\bar{m}/dt)$, leads to the breakup law which relates the product drop size to the breakup time as determined by the TAB model.

$$\frac{d\bar{m}}{dt} \; = \; -3K_{br}\bar{m} \tag{40}$$

The breakup constant K_{br} depends on the breakup regime and is given by parent drop properties only. Bag breakup occurs if $We \; = \; We_t$ and stripping breakup happens if $We \; > \; We_t$. And it is given by

$$K_{br} = k_1\omega \quad if\ We \le We_t \quad or$$
$$K_{br} = k_2\omega\sqrt{We} \quad if\ We > We_t \tag{41}$$

The values for We_t, k_1 and k_2 have been determined experimentally and has been set to $k_1 \approx k_2 = 1/4.5$ and $We_t = 80$.

In this model, a uniform product droplet size distribution is assumed. It is also noted that the choice of uniform distribution is not expected to be realistic but may produce good approximations when averaged over many drop breakups, because parent drops of different sizes and Weber numbers will in general yield a wide range of duct droplet sizes. With this assumption, Eq. (40) becomes

$$\frac{r}{a} = e^{-K_{br}t} \tag{42}$$

where a and r are the radii of the parent and product drops, respectively.

After breakup of a parent drop, the initial deformation parameters of the product droplets are set to $y(0) = \dot{y}(0) = 0$. Also, the product droplets are initially supplied with a velocity component perpendicular to the path of the parent drop with a value $v_T = A\dot{x}$, where A is a constant determined from the following energy balance consideration. The energy of the parent drop is the sum of the surface tension energy and the droplet deformation energy. The second is computed as the product of the aerodynamic drag and the drop deformation at the stagnation point, estimated to be $5a/9$. This leads to

$$E_{parent} = 4\pi\sigma a^2 + 5\pi c_d\rho_g a^3|U|^2/18 \tag{43}$$

And the energy of the product droplets in the frame of reference of the parent drop is given by

$$E_{product} = 4\pi\sigma a^3/r_{SMR} + A^2\pi\rho_l a^5\dot{y}^2/6 \tag{44}$$

where the Sauter mean radius, r_{SMR}, enters via the relation $\bar{r}^2 = a^3/r_{SMR}$. From Eqs. (43) and (44) one obtains the relation

$$A^2 = 3[1 - 1/r_{SMR} + 5c_dWe/72]\omega^2/\dot{y}^2 \tag{45}$$

where $\omega^2 = \frac{8\sigma}{\rho_l a^3}$. Tanner [7-8] analysis yields an approximate value of 0.69 for A showing that only 70% of the parent drop deformation velocity goes into the normal velocity component of the product droplets, where as it is 100% in the standard TAB model. Also, the characteristic time, τ $(= \frac{1}{K_{br}})$, for breakup in Eq. (42) for an inviscid liquid ($\mu_l = 0$) is given by $\alpha_1\sqrt{\frac{\rho_l a^3}{\sigma}}$ $if\ We \le We_t$ or $\alpha_2\sqrt{\frac{\rho_l}{\rho_g}}\frac{a}{|U|}$ $if\ We > We_t$, where the suggested values are for $\alpha_1 = (\sqrt{8}k_1)^{-1}$ and $\alpha_2 = (\sqrt{8}k_2)^{-1}$.

The application of the ETAB model in the simulation of a high pressure liquid jet breakup can be found in [7-8].

5 RESULTS & DISCUSSION

Here we summarize some results from several test runs performed within the context of a single McDonnell-Samuelsen case [23]. However, it is also noteworthy that the validation results for the McDonnell-Samuelsen case were already reported in [4]. In the calculations of [4] the initial droplet conditions were specified from known experimental data. And the comparisons involving both gas and drop velocities, drop size distributions, and gas temperatures showed reasonable agreement with the available experimental data. The purpose of the present exercise is not for validation but it was designed primarily as a debugging platform for assessing the differences between various models. The designed matrix consisted of a total of twenty test runs resulting from various combinations of available models for primary atomization and secondary droplet breakup.

The schematic of the experimental facility used at UCI (University of California, Irvine) is shown in Fig. 1. It made use of the RSA (Research Simplex Atomizer) which was manufactured by Parker and Hannifin. The injector has a nominal spray angle of 85^0 (full angle) and the spray liquid was methanol ($\rho_l = 770kg/m^3$, $\sigma = 22.2g/s^2$, $\nu_l = 2.5m^2/s$). The reported methanol and air mass flow rates were 1.26 and 1.32 g/s, respectively. The spray was injected downwards from the center of a 495 x 495 mm square duct and air was pulled through the top of the duct by a blower at a bulk velocity of 0.8 m/s in order to provide adequate entrainment needs. Both the droplet and gas-phase velocities as well as the droplet sizes were measured by making use of a two-component PDI (Phase Doppler Interferometry), and the gas-phase temperatures were measured by using a traversing hot-wire thermocouple. Using the setup shown in Fig. 1, several measurements involving the gas-phase velocity, droplet size and velocity, droplet number flux, and mean gas-phase temperatures were reported at different axial locations starting from 2.5 cm. The back-lit experimental photograph of the spray are shown in Fig. 2.

In all the calculations, the computations were performed on a 2D axisymmetric grid of 1850 triangular elements. The calculations were advanced until a steady state solution was reached by making use of the following time steps: Δt_g (= local time step used in the flow solver, s) was determined based on a CFL number of 1, $\Delta t_{injection}$ (time-step at which a new group of droplets is introduced) = 1.0 ms, and Δt_k (time step used in the spray solver) = 0.01 ms. The initial gas conditions were prescribed from the experimental data taken at 2.5 cm. Based on the reported experimental data, the following conditions were assumed for the injector: the droplet injection velocity 45m/s, the nozzle diameter 0.1 mm, and the liquid temperature 298 K.

5.1 The calculations with the droplet initial conditions taken from the experimental data

The global features of a reacting spray flow-field are shown in Fig. 3a-3d. Here, a composite view is presented in the form of both drop locations, mean gas temperatures and gas velocity vectors. The solid white circles show the location of the droplets. The shaded contour lines show the temperature distribution, and the arrows denote the gas velocity vectors. The droplet sizes range from few microns to 140 microns. Most of the smaller droplets are taken out of the computation once they loose more than 99% of their initial mass due to evaporation. As expected, some of the larger droplets leave the domain through the right exit boundary. The gas temperature distribution ranges between 564 to 2325 K. The results in Fig. 3a are similar to those reported in [4] from the non-PDF computations where combustion takes place in a predominantly vaporization-controlled reaction regime after originating next to the inflow boundary.

Figs. 3b-3d show the results obtained from the use of the Rayleigh-Taylor, TAB, and ETAB secondary breakup models, respectively. The effect of the secondary breakup mechanism is primarily seen to further broaden the high temperature region near the inflow boundary. And the results from both of TAB and ETAB can be seen to be nearly identical. In this case, all the secondary breakup models seem to have only a modest effect on the overall spray performance.

5.2 The calculations with the sheet-breakup primary atomization model

None of the primary atomization models were designed specifically for the simplex injector type of application. But the primary atomization model that comes closest for this kind of injector representation is the high pressure swirl application of the sheet-breakup primary atomization model described in Section 3.1.1.

The results from the sheet-breakup primary atomization model with various secondary breakup models are shown in Figs. 4a-d. This primary atomization model seems to produce a hollow cone spray and overemphasize this representation as it shifts the location of the high temperature region radially outwards into the middle of the spray away from the centerline (Figs. 4a-d). Originating from the middle of the spray, a high temperature region spreads further downstream centered around the middle of the spray. The results from Figs. 4a & 4c-4d are similar and the additional effect of either TAB or ETAB secondary breakup models seem to be modest. In all the cases considered, the Rayleigh-Taylor secondary breakup has established a definite pattern by favoring a more rapid breakup into smaller droplets and, thereby, promoting a faster

rate of liquid evaporation when compared with either TAB or ETAB. This effect is evident by the further reduction achieved in the axial flame stand-off distance with the Rayleigh-Taylor breakup when compared with either TAB or ETAB. The predicted axial flame stand-off distance is about 6.5 cm with the Rayleigh-Taylor secondary breakup model and the results from Figs. 4a & 4c-4d seem to overpredict the axial flame stand-off distance (about 13 cm) even more. The axial stand-off distances in all Figs. 4a-4d are overpredicted as the experimental data of McDonnell and Samuelsen shows for it to be 2.5 cm.

5.3 The calculations with the air blast primary atomization model

The air blast primary atomization also seems to produce a hollow cone spray and overemphasize this representation as it shifts the location of the high temperature region radially outwards into the middle of the spray away from the centerline (Figs. 5a-d). Originating from the middle of the spray, a high temperature region spreads further downstream centered around the middle of the spray. Also, the axial flame stand-off distances are overpredicted compared to the experimental observation of 2.5 cm. While the overall behavior is similar to the sheet-breakup primary atomization, the axial flame stand-off distances are better predicted in Figs. 5a, & 5c-d compared to Figs. 4a, & 4c-d.

5.4 The calculations with the blob jet primary atomization model

For this primary atomization model, the results are only shown for a non-reacting spray as the calculations other than the Rayleigh-Taylor secondary breakup model couldn't support a spray flame (Figs. 6a-6d). Here the spray is represented by a solid cone spray with an initial half cone angle of 45^0. Initially, a specified number of size 100 μm droplets (mono-disperse) called blobs were injected and they were dispersed uniformly across a half cone angle of 45^0. The injected blobs within the intact liquid core move initially in a straight line before the jet breakup occurs [5,16,9]. After the intact core breakup, new product droplet parcels are produced from the breakup of the blobs [9]. And the size of the initial product drops could even exceed the size of the parent drops.

Judging from the spray representation, the spray angle is well calculated. However, the spacing between different bands of droplets in Fig. 6a clearly reflects the effect of the present discrete injection method. Each separate band represents a group of particles injected at a different injection time interval, $\Delta t_{injection}$. The distancing gets smaller as we move towards the outflow boundary because of the resulting droplet deceleration due to drag. However, the axial location for the last group of injected drops can be estimated by knowing the specified droplet injection time, $\Delta t_{injection}$, and the initial injection velocity. Finally, all the droplets exit out of domain from the outflow boundary. Figs. 6b-d show the results from the Rayleigh-Taylor, TAB, and ETAB droplet secondary breakup models, respectively. While the results from both of TAB and ETAB are very similar, they, however, differ significantly from the Rayleigh-Taylor secondary breakup. For some reason, Rayleigh-Taylor secondary breakup seemed to produce droplets of smaller sizes when compared with either of TAB or ETAB. The smaller droplets so produced are swept away axially further downstream by the surrounding gas. In the reacting calculations not shown here most of the product droplets so produced by the Rayleigh-Taylor breakup seemed to evaporate rather quickly after the secondary breakup criterion was applied. On the other hand, both of TAB and ETAB produce a nicely dispersed solid cone spray as can be seen in Figs. 6c-d. After an axial distance of about 10 cm, they also seem to produce spray drops as in the second wind jet breakup regime of Reitz and Bracco [5] with sizes smaller than the nozzle diameter. However, further effects of combined evaporation and mixing don't appear to be fast enough to support a flame.

5.5 The calculations with the BLS primary atomization model

The results in Figs. 7a-d from the BLS method are similar to those obtained from the blob jet primary atomization model with few exceptions. Unlike the previous case, the results from Figs. 7a are also similar to the results from TAB and ETAB (Figs. 7c-d). Also, the results in 7a are all similar to those from Fig. 6a. The results from the Rayleigh-Taylor secondary breakup in both of the blob jet and BLS cases are similar

(Fig. 7b and Fig. 6b) to the extent that the Rayleigh-Taylor breakup produces product droplets which are small. The droplets so produced are swept away axially further downstream by the surrounding gas. However, the BLS method seems to delay the onset of secondary breakup effects further downstream.

6 CONCLUSIONS

We have successfully integrated the CFDRC/UW atomization module into NCC. Complete details of various primary atomization models as well as secondary droplet breakup models contained in the atomization module are provided. The differences between various atomization models on the overall performance of a single reacting spray case were investigated. The designed test matrix encompassed all the possible joint combinations of various primary atomization and secondary droplet breakup models. A brief summary of the results are as follows:

- The calculations with the droplet initial conditions taken from the experimental data showed that the effect of various secondary breakup models on the global structure of a reacting spray seems to be modest for the case investigated.
- Both the sheet breakup and air blast primary atomization models yielded similar results but the structure of the flame differs significantly from the experimentally observed flame. The results also overpredicted the axial flame stand-off distances by a considerable measure.
- Both the blob-jet and BLS primary atomization models produced similar results but the calculations other than the Rayleigh-Taylor secondary breakup model couldn't support a spray flame.
- Between the three secondary droplet breakup models, the results from both TAB and ETAB are mostly similar but the Rayleigh-Taylor secondary breakup mechanism seemed to produce droplets which are smaller.
- The comparisons with the experimental data suggests a definite need for further improvements in the modeling of a spray flame produced by a simplex fuel injector.

8 REFERENCES

1. M.S. Raju, "LSPRAY-II: A Lagrangian Spray Module," NASA/CR-2004-212958, Glenn Research Center, NASA, Ohio-44135, March 2004.
2. M.S. Raju, "EUPDF-II: An Eulerian Joint Scalar Monte Carlo PDF Module - User's Manual," NASA/CR-2004-213073, Glenn Research Center, National Aeronautics and Space Administration, Ohio-44135, March 2004.
3. M.S. Raju, "Current Status of the Use of Parallel Computing in Turbulent Reacting Flows: Computations Involving Sprays, Scalar Monte Carlo Probability Density Function & Unstructured Grids," Advances in Numerical Heat Transfer, vol. 2, ch. 8, pp. 259-287, 2000.
4. M.S. Raju, "On the importance of Chemistry/Turbulence Interactions in Spray Computations," Numerical Heat Transfer, Part: B: Fundamentals, Vo. 41, pp. 409-432, 2002.

5. Reitz, R.D., & Bracco, F.V., "Mechanism of Atomization of a Liquid Jet," Phy. Fluids, Vol. 25, ch. 10, Oct., 1982.

6. O'Rourke, P.J., and Amsden, A.A., "The TAB Method for Numerical Calculation of Spray Droplet Breakup," SAE Technical Paper 872089, 1987.

7. Tanner, F.X., "Liquid Jet Atomization and Droplet Breakup Modeling of Non-evaporating Diesel Fuel sprays," SAE Technical Paper 970050, 1998. Also SAE 1997 Transactions: Journal of Engines, Vol. 106, Sec. 3, pp. 127-140, 1998.

8. Tanner, F.X., "A Cascade Atomization and Drop Breakup Model for the Simulation of High-Pressure Liquid Jets," SAE Paper 2003-01-1044, 2003.

9. Reitz, R.D., "Modeling Atomization Processes in High-Pressure vaporizing Sprays," Atomization and Spray Technology, Vol. 3, pp. 309-337, 1987.

10. Reitz, R.D., and Diwakar, R. "Structure of High-Pressure Fuel Sprays," SAE paper 870598, 1987.

11. Khosla, S., and Crocker, D.S., "CFD Modeling of the Atomization of Plain Jets in Cross Flow for Gas Turbine Applications"' IGTI Turbo Expo: Combustion & Fuels, GT2004-54269, Vienna, Austria, June 2004.

12. Schmidt, D.P., Nouar, I., Senecal, P.K., Hoffman, J., Rutland, C.J., Martin. J., & Reitz, R.D., "Pressure-Swirl Atomization in the Near Field," 1999 SAE Congress, SAE 1999-01-0496.

13. Senecal, P.K., Schmidt, D.P., Nouar, I., Rutland, C.J., & Reitz, R.D., "Modeling High Speed Viscous Liquid Sheet Approximation," 1998.

14. Dombrowski, N., & Hooper, P.C., "The Effect of Ambient Density on Droplet Formation in Sprays," Chem. Eng. Sci. vol. 17, pp. 291, 1962.

15. Dombrowski, N., & Johns, W.R., "The Aerodynamic Instability and Disintegration of Liquid Sheets," Chem. Eng. Sci. vol. 1718, pp. 203, 1963.

16. Reitz, R.D., "Computer Modeling of Sprays," Spray Technology Short Course, Pittsburg, PA May 7, 1997.

17. Taylor, G.I., "The instability of Surfaces When Accelerated in a Direction Perpendicular to Their Planes," Proc. Royal Soc., A, Vol. 201, pp.192-196, 1950.

18. Hwang, S.S., Liu, Z., and Reitz, R.D., "Breakup Mechanisms and Drag Coefficients of High-Speed Vaporizing Liquid Drops," Atomization and Sprays, Vol. 6, pp. 353-376, 1996.

19. Liu, A.B., Mather, D., and Reitz, R.D., "Modeling the Effects of Droplet Drag and Breakup on Fuel sprays," SAE Technical paper 930072, 1993.

20. Liu, A.B., and Reitz, R.D., "Mechanisms of Air-Assisted Liquid Atomization," Atomization and Sprays, Vol. 3, pp. 55-75, 1993.

21. Patterson, M.A., and Reitz, R.D., "Modeling the Effects of Fuel Characteristics on Diesel Engine Combustion and Emission," SAE 980131,1998.

22. Amsden, A.A., O'Rouke, P.J., and Butler, T.D., "KIVA II: A Computer Program for Chemically Reactive Flows With Sprays," Technical report LA-11560-MS, Los Alamos laboratory, May 1989.

23. V.G. McDonnell and G.S. Samuelsen, An Experimental Data Base for the Computational Fluid Dynamics of Reacting and Nonreacting Methanol Sprays, J. Fluids Engineering, vol. 117, pp.145-153, 1995.

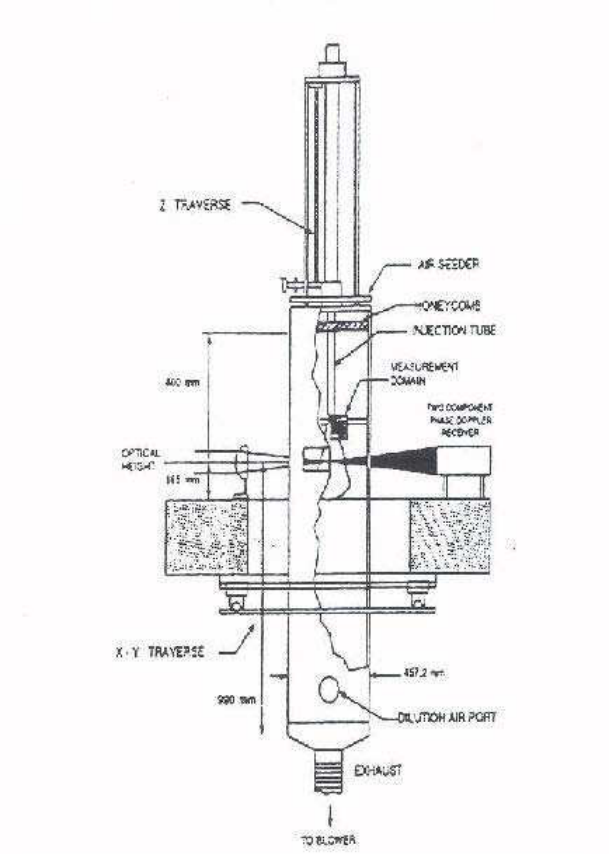

Fig. 1 Schematic of the spray burner facility (McDonell and Samuelsen).

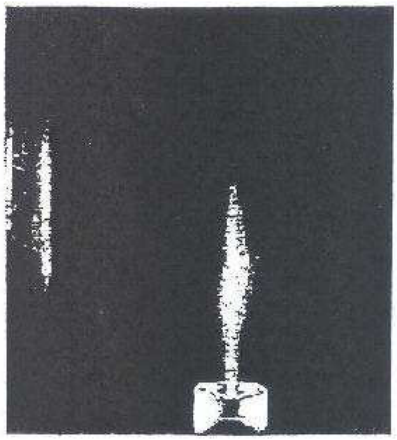

(a) Case 1, reacting and no-swirl

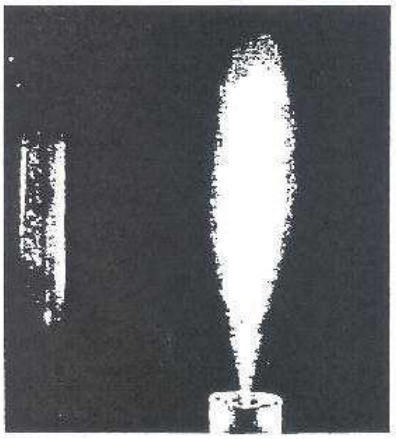

(b) Case 2, non-reacting and no-swirl

Fig. 2 Backlit photographs of sprays (McDonell and Samuelsen).

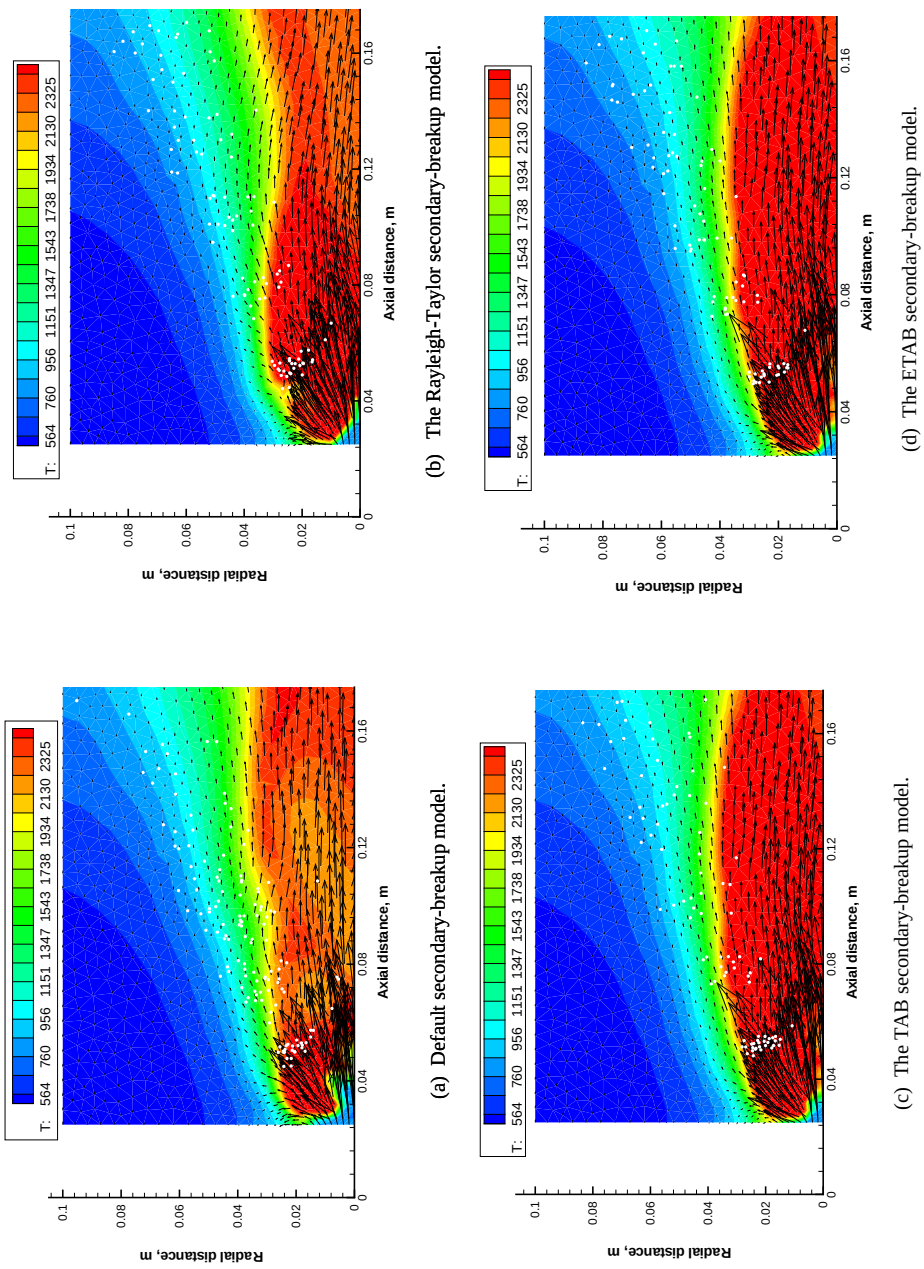

(a) Default secondary-breakup model.

(b) The Rayleigh-Taylor secondary-breakup model.

(c) The TAB secondary-breakup model.

(d) The ETAB secondary-breakup model.

Fig. 3 Global structure of a spray flame with the droplet initial conditions taken from the experimental data.

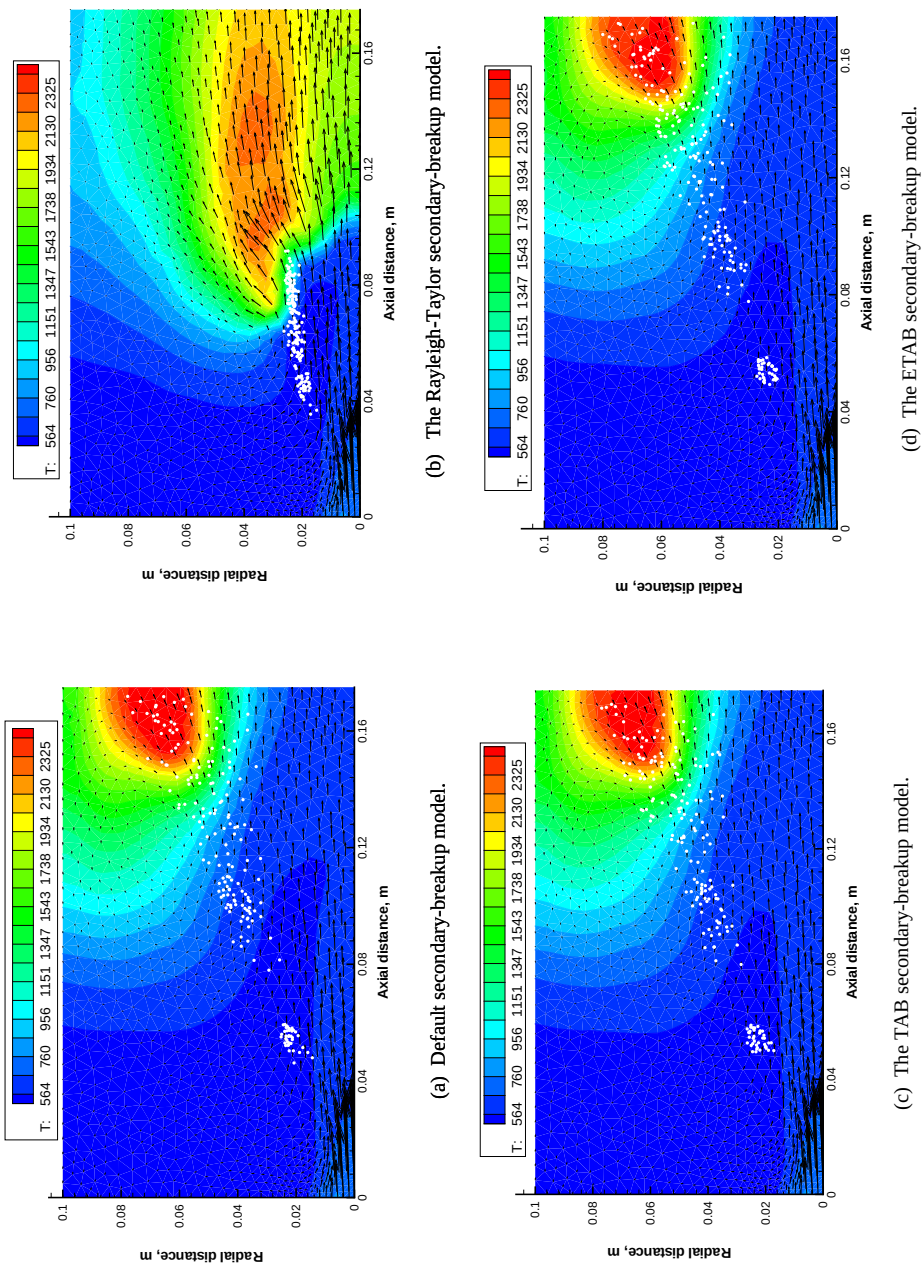

(a) Default secondary-breakup model.

(b) The Rayleigh-Taylor secondary-breakup model.

(c) The TAB secondary-breakup model.

(d) The ETAB secondary-breakup model.

Fig. 4 Global structure of a spray flame with the sheet-breakup primary atomization model.

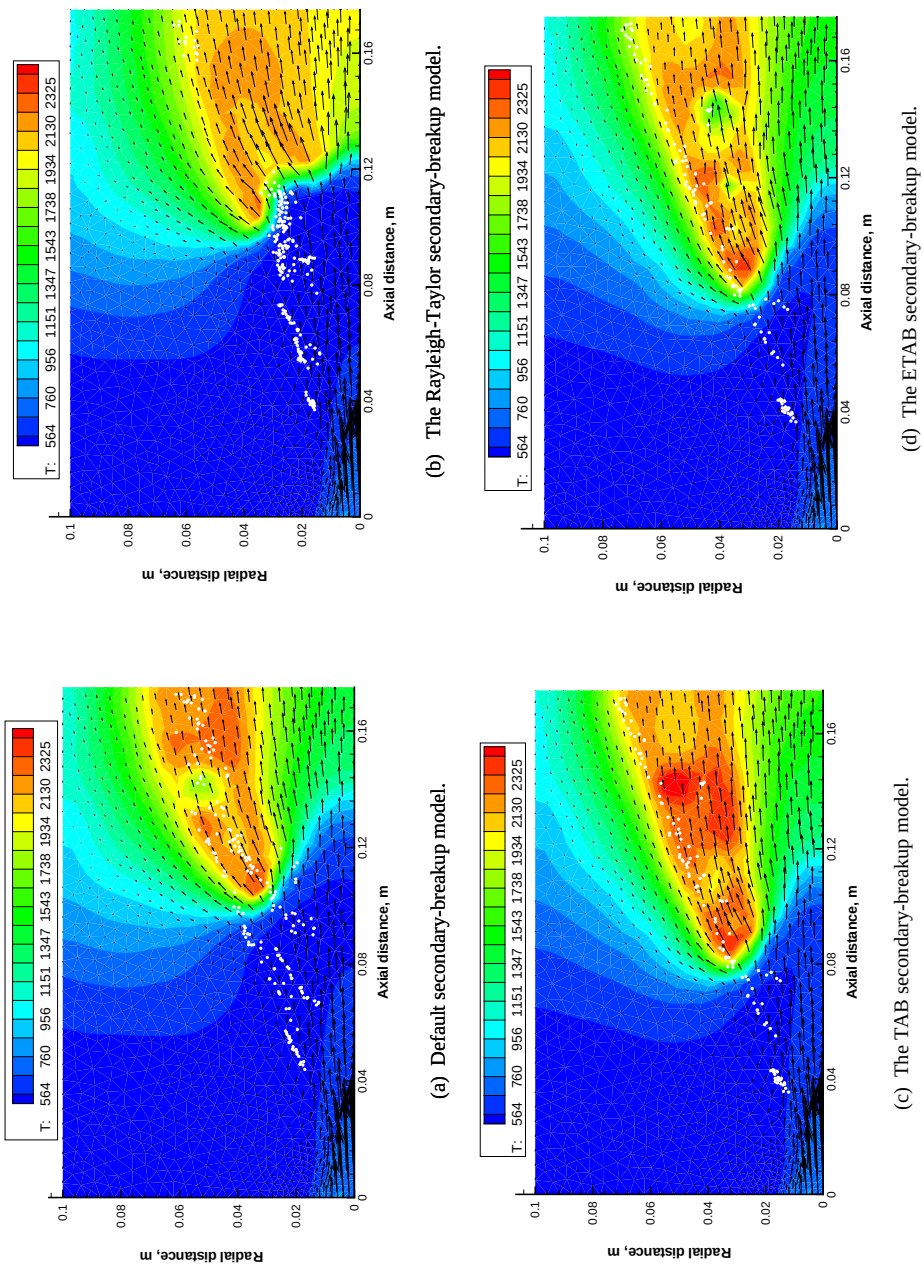

(a) Default secondary-breakup model.

(b) The Rayleigh-Taylor secondary-breakup model.

(c) The TAB secondary-breakup model.

(d) The ETAB secondary-breakup model.

Fig. 5 Global structure of a spray flame with the air-blast primary atomization model.

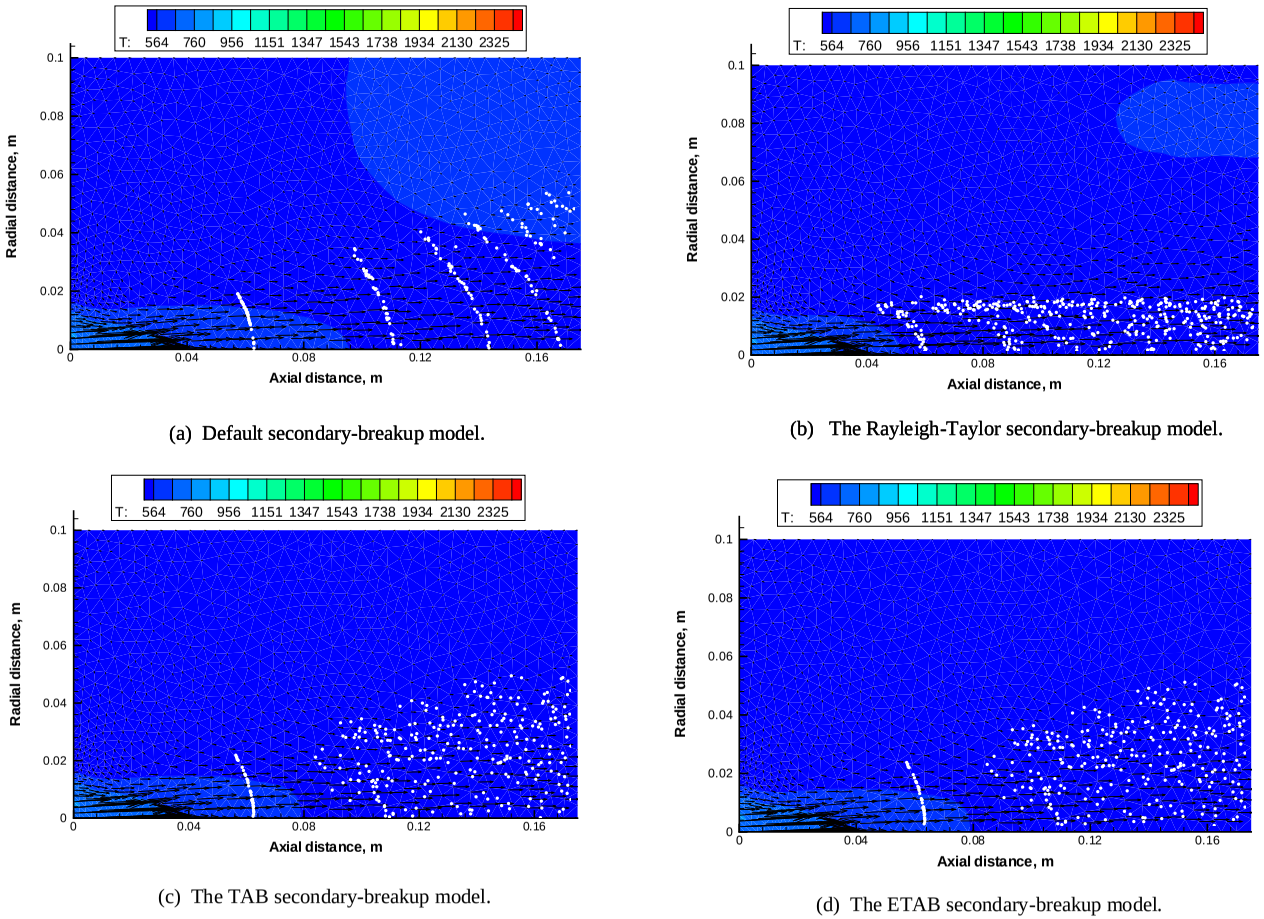

(a) Default secondary-breakup model.

(b) The Rayleigh-Taylor secondary-breakup model.

(c) The TAB secondary-breakup model.

(d) The ETAB secondary-breakup model.

Fig. 6 Global structure of a spray flame with the blob-jet primary atomization model.

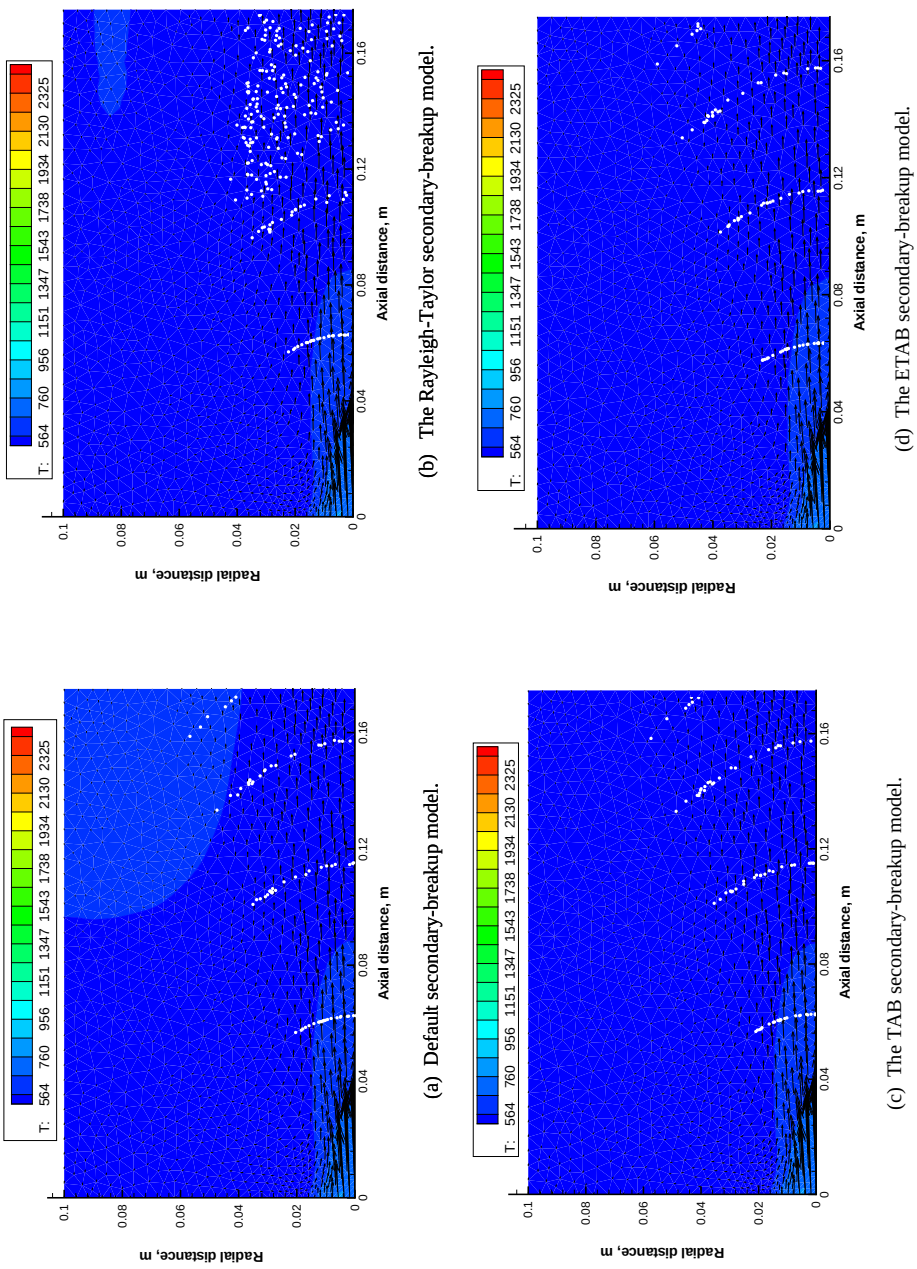

(a) Default secondary-breakup model.

(b) The Rayleigh-Taylor secondary-breakup model.

(c) The TAB secondary-breakup model.

(d) The ETAB secondary-breakup model.

Fig. 7 Global structure of a spray flame with the BLS primary atomization model.

REPORT DOCUMENTATION PAGE

Form Approved
OMB No. 0704-0188

1. AGENCY USE ONLY (*Leave blank*)	2. REPORT DATE	3. REPORT TYPE AND DATES COVERED
	November 2005	Final Contractor Report

4. TITLE AND SUBTITLE

Numerical Investigation of Various Atomization Models in the Modeling of a Spray Flame

5. FUNDING NUMBERS

WBS–22–714–20–22
NAS3–00145

6. AUTHOR(S)

M.S. Raju

7. PERFORMING ORGANIZATION NAME(S) AND ADDRESS(ES)

QSS Group, Inc.
21000 Brookpark Road
Cleveland, Ohio 44135

8. PERFORMING ORGANIZATION REPORT NUMBER

E–15389

9. SPONSORING/MONITORING AGENCY NAME(S) AND ADDRESS(ES)

National Aeronautics and Space Administration
Washington, DC 20546–0001

10. SPONSORING/MONITORING AGENCY REPORT NUMBER

NASA CR—2005-214033
AIAA–2006–0176

11. SUPPLEMENTARY NOTES

Prepared for the International Conference on Computational and Experimental Engineering and Sciences cosponsored by the North Carolina A&T University, Simulation Technology Services Private, Ltd., U.S. Army Research Office, U.S. Army Asian Research Office, U.S. Air Force Asian Office of Aerospace Research and Development, The Indian National Academy of Engineering, and the National Science Foundation, Chennai, India, December 1–6, 2005; and the 44th Aerospace Sciences Meeting and Exhibit sponsored by the American Institute of Aeronautics and Astronautics, Reno, Nevada, January 9–12, 2006. Project Manager, Nan-Suey Liu, Propulsion Systems Division, NASA Glenn Research Center, organization code RTB, 216–433–8722.

12a. DISTRIBUTION/AVAILABILITY STATEMENT

Unclassified - Unlimited
Subject Categories: 02, 07, 08, 20, and 24

Available electronically at http://gltrs.grc.nasa.gov

This publication is available from the NASA Center for AeroSpace Information, 301–621–0390.

12b. DISTRIBUTION CODE

13. ABSTRACT ***(Maximum 200 words)***

In modern aircraft and rocket engine combustors, the atomization characteristics of a fuel nozzle as defined by the spray dispersion angle, droplet-size and velocity distributions, and fuel vaporization play an important role in determining the combustor performance, e.g. the combustion efficiency, ignition and lean blowout conditions, exit temperature pattern, and emissions. The success of any spray calculation depends a great deal on the correct specification of the initial droplet conditions. However, the modeling of the atomization process is a very challenging task as it is influenced by a variety of factors: the aerodynamic liquid-gas interaction, the inner nozzle disturbances, the nozzle geometry, and the thermo-physical properties of fuel. So far in our previous spray computations, we have relied on either known experimental data or data generated from widely-used correlations in specifying the initial droplet conditions. In order to reduce some uncertainty associated with the specification of the initial droplet conditions, we have undertaken the task of integrating an atomization module into our spray calculation procedure of the national combustion code (NCC). The atomization module contains the following primary atomization models: sheet breakup; air blast; blob jet; and BLS (Boundary-Layer Stripping), together with the following secondary droplet breakup models: Rayleigh-Taylor; TAB (Taylor Analogy Breakup); and ETAB (Enhanced Taylor Analogy Breakup). The paper provides complete details of various models contained in the atomization module. And it also summarizes the results from the study conducted to investigate the effect of various atomization models in the modeling of a spray flame.

14. SUBJECT TERMS

Spray combustion; Modeling; Atomization; Turbulent combustion; CFD; Monte Carlo PDF

15. NUMBER OF PAGES

28

16. PRICE CODE

17. SECURITY CLASSIFICATION OF REPORT	18. SECURITY CLASSIFICATION OF THIS PAGE	19. SECURITY CLASSIFICATION OF ABSTRACT	20. LIMITATION OF ABSTRACT
Unclassified	Unclassified	Unclassified	